


FULL PAPER

Open Access



# Reconstruction of the deformation history of an active fault: implications from the Atera Fault, Central Japan

Horst Zwingmann<sup>1\*</sup> , Masakazu Niwa<sup>2</sup>, Andrew Todd<sup>3</sup> and Martin Saunders<sup>4</sup>

## Abstract

Atera Fault clay gouges were collected for age dating near Kawaue, Nakatsugawa City, Central Japan, and the results integrated within its complex geological history. The results form an internally consistent data set constrained by extensive geochronological data (AFTA, ZFTA, CHIME) and support the application of gouge dating in constraining timing of brittle deformation in Central Japan. The Atera illite age data complete recently obtained limited illite fault gouge age data from underground exposure in the Toki Granite; the new illite age data are identical within error. The age of the heterogenous welded tuff breccia zone (Atera 1) ranges from  $40.6 \pm 1.0$  Ma to  $60.0 \pm 1.4$  Ma, whereas ages of the fault core gouge sample (Atera 2) range from  $41.8 \pm 1.0$  Ma to  $52.7 \pm 1.2$  Ma. The finest  $< 0.1 \mu\text{m}$  fraction of the fault breccia and fault core gouge yield ages around 41 Ma, identical within error. The new illite age data indicate brittle faulting and a following geothermal event occurring in the Paleogene–Eocene, similar to the nearby Toki Granite area and confirm they were both synchronous with a post-intrusive pluton exhumation. The Atera Fault illite age data provide additional insights into an integrated, regional-scale record of the tectonic displacement of Central Japan and might be influenced by large-scale tectonic processes such as the Emperor sea mount kink around 55 to 46 Ma with fault initiation around 50 Ma and brittle fault cessation or reactivation around 40 Ma in the Eocene.

**Keywords** Brittle fault, Illite, K-Ar dating, Atera fault, Japan

\*Correspondence:

Horst Zwingmann

horst@kueps.kyoto-u.ac.jp

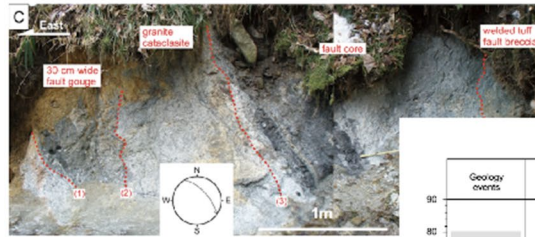
Full list of author information is available at the end of the article



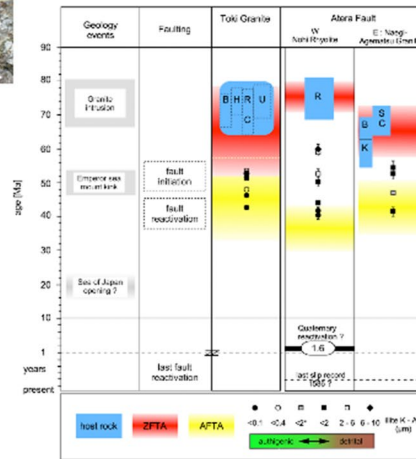
© The Author(s) 2024. **Open Access** This article is licensed under a Creative Commons Attribution 4.0 International License, which permits use, sharing, adaptation, distribution and reproduction in any medium or format, as long as you give appropriate credit to the original author(s) and the source, provide a link to the Creative Commons licence, and indicate if changes were made. The images or other third party material in this article are included in the article's Creative Commons licence, unless indicated otherwise in a credit line to the material. If material is not included in the article's Creative Commons licence and your intended use is not permitted by statutory regulation or exceeds the permitted use, you will need to obtain permission directly from the copyright holder. To view a copy of this licence, visit <http://creativecommons.org/licenses/by/4.0/>.

## Graphical Abstract

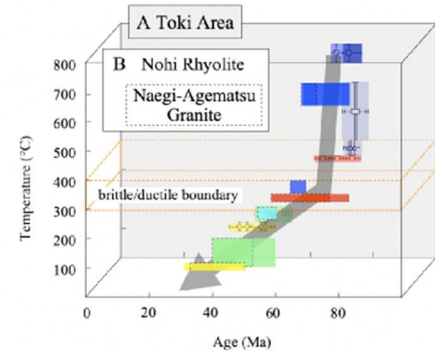
### 1. Field area



### 2. Geochronology



### 3. Thermal history



## Introduction

Clay fault gouges are present in active brittle faults formed under near surface conditions (e.g., Scholz 2002). Active fault zones often document numerous geological processes ranging from the disintegration of host rocks with subsequent grain-size reduction and authigenesis of clay minerals (chlorite, smectite, illite) and muscovite.

In addition, secondary heating and melting of host rocks by frictional deformation (pseudotachylytes) and fault-related fluid flow might result in mineral vein formation (e.g., Holdsworth et al. 1997; Tagami 2012). Authigenic illite in fault gouges can reliably constrain the timing of fault activity by K–Ar,  $^{40}\text{Ar}/^{39}\text{Ar}$  and Rb–Sr dating (see summaries in Vrolijk et al. 2018; Tsukamoto et al. 2020). Despite more than 50 years of research, the timing of slip on brittle faults in the Earth's upper crust are difficult to constrain and radiometric dating of fault zones remains challenging. Over the last decade, K–Ar data of authigenic illite formed in brittle fault zones are integrated with apatite fission-track (AFTA) and zircon fission-track (ZFTA) data as the frictional heating caused by fault motion can partially or totally reset the “clock” of the dating methods (Zwingmann et al. 2004, 2010; Zwingmann and Mancktelow 2004; Tagami 2005, 2012; Yamasaki et al. 2013). Timing of fault formation and its corresponding geofluid sources can be investigated

through the robust isotopic memory of neo-crystallized authigenic clay minerals as its crystal structure includes H (as OH) and K, enabling constraint of fluid sources through H isotope analysis and timing through Argon dating (e.g., Hetzel et al. 2013; Mancktelow et al. 2015, 2016; Lynch and van der Pluijm 2016; Heinecke et al. 2019). Limited studies apply a whole range of dating methods such as K–Ar,  $^{40}\text{Ar}/^{39}\text{Ar}$ , and Rb–Sr dating of syntectonic fault-related illite (e.g., Middleton et al. 2014; Uysal et al. 2020). U–Pb dating of carbonate geochronology can provide direct timing constraints for geological processes involving diagenesis, fluid flow, brittle faulting via carbonate slickenfibers and vein-related tectonic processes (e.g., Mottram et al. 2020), but was applied prior to in situ U–Pb dating of low-U fault-related carbonate (e.g., Nuriel et al. 2017; Roberts et al. 2020). However, some fault gouges lack calcite and quartz veins developed by fluid interaction and therefore cannot be investigated by in situ U–Pb geochronology (i.e., Kemp et al. 2019). Most studies focus on the thermal effect on clay gouge during brittle deformation, as fault zones might reactivate numerous times over their complex geological history, from formation to last slip event and subsequent grain-size reductions during multiple faulting events might affect its isotopic signature (e.g., Zwingmann et al. 2019). Clay fault gouge associated with the Atera Fault

were collected within this study for K–Ar dating from a well-exposed river section near Kawaue, Nakatsugawa city, Central Japan (Fig. 1).

### Geological framework

Active inland faults are widespread in Japan and investigations are important for earthquake forecasting and seismic hazard assessments (Toda 2016). Comprehensive geological summaries of fault zones in Japan and the Geology of Japan, including the study area, can be found elsewhere (Moreno et al. 2016). The study area is located in Central Japan approximately 70 km NE of Nagoya (Fig. 1). The Atera Fault is one of numerous large strike-slip left-lateral active faults in Central Japan and extends for ca. 55 km from Nakatsugawa City to Gero City in Gifu Prefecture in a general NW to SE trend (Takagi et al. 2005). As discussed by Niwa et al. (2009), the outcrop comprises fault breccia, clay-rich fault gouge, and cataclasite with significant asymmetry due to different protolith lithology. The Atera Fault zone outcrop record several stages of deformation which are based on a field-based and microstructural study by Niwa et al. (2009). The last recent displacement of the Atera Fault occurred

during a large earthquake in 1586 (Toda et al. 1996; Niwa et al. 2009).

Central Japan has a long and complex deformation history documented by neotectonic processes and interactions between topography and erosion. Surface exposures enable the study of fault gouges which are often poorly preserved due to extended weathering. The ages of the basement and host rocks in the study area are well constrained and supplemented by a large set of regional thermochronological data. However, only a few studies on localized retrograde authigenic clay mineral formation in discrete fault zones in Japan have been reported in the literature (Yamasaki et al. 2013), although such brittle faults are widespread and similar to studies reported within the European Alps (Zwingmann and Mancktelow 2004; Zwingmann et al. 2010a).

The investigated fault outcrops are located in Kawaue, Nakatsugawa city (Fig. 1c; Niwa et al. 2009; 2015). K–Ar dating of Atera Fault gouge is discussed in a report by Yamada et al. (1992) for limited  $< 2 \mu\text{m}$  clay fractions from different locations. The mineral compositions of the investigated gouges by Yamada et al. (1992) were determined by qualitative XRD analysis indicating mica clay

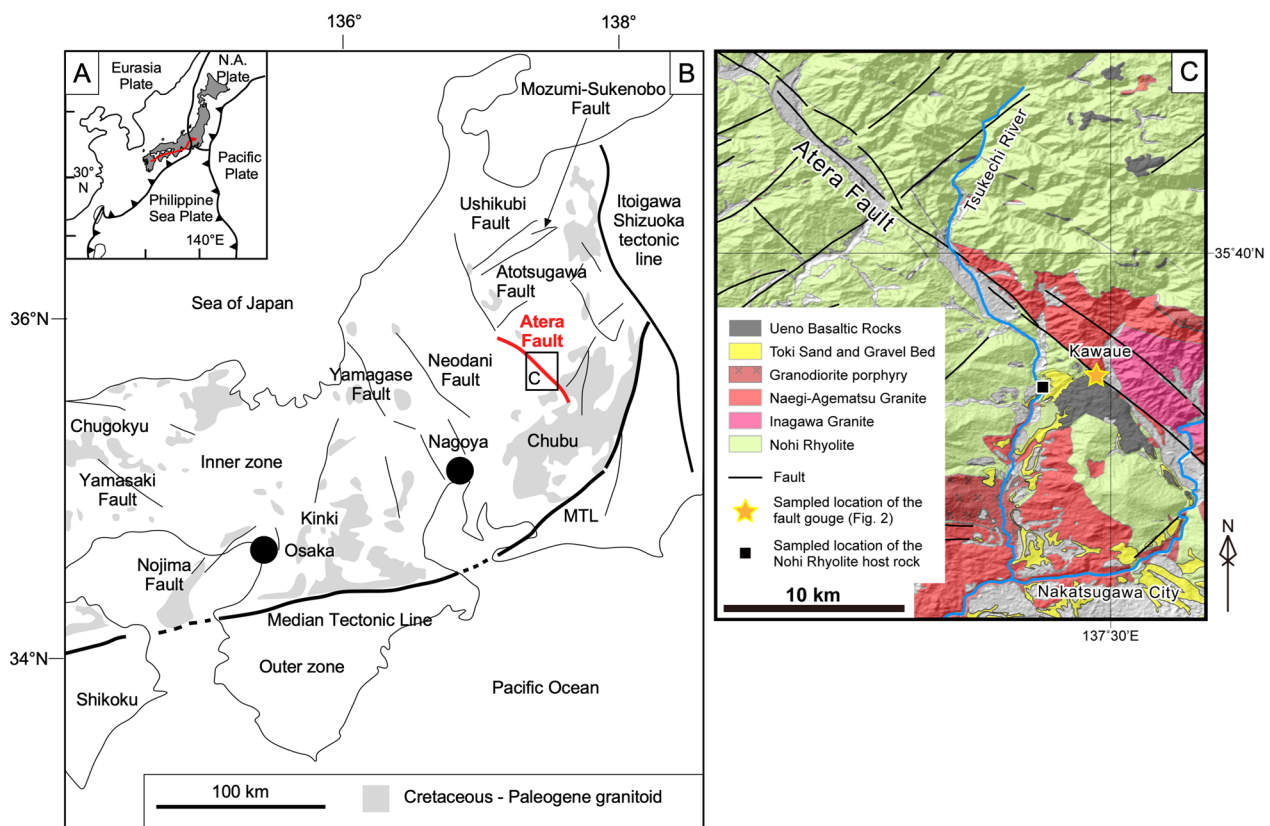


**Fig. 1** Study area. **A** Location map Japan with Median Tectonic Line (MTL) shown in red, N.A. North American Plate, **B** fault zones in Central Japan (modified from Takagi et al. 2005), **C** Atera Fault local geology

mineral in addition to montmorillonite, quartz, kaolinite, chlorite, and feldspar. The reported ages range from  $22.9 \pm 0.8$  Ma to  $54.6 \pm 1.8$  Ma covering a large age range of 33.7 Ma for 7 samples. Based on a biotite K–Ar age from host rock granite at the same location, the  $22.9 \pm 0.8$  Ma fault gouge sample suggests alteration. According to Niwa et al. (2009), the Kawaue basement comprises the Inagawa Granite, the Gero Ash-Flow sheet of the Nohi Rhyolite, the Naegi–Agematsu Granite, the Toki Sand and Gravel Bed, and the Ueno Basaltic Rocks (Fig. 2). The Inagawa Granite relates to the extensive Ryoke Granites, which intruded during the Cretaceous and its age was constrained by CHIME analyses in two localities with ages of  $82.6 \pm 1.8$  Ma and  $81.9 \pm 1.4$  Ma ( $2\sigma$ ) which are identical within error (Suzuki and Adachi 1998). The Gero Ash-Flow Sheet represents a welded tuff with a younger  $75.2 \pm 6.2$  Ma ( $1\sigma$ ) Rb–Sr whole-rock isochron age (Shirahase 2005; Yamada and Koido 2005) and is part of the Late Cretaceous Nohi Rhyolite composite volcanism in Central Japan (Yamada et al. 2005). The Naegi–Agematsu Granite was dated at  $67.2 \pm 3.2$  Ma (CHIME,  $2\sigma$ ) (Suzuki et al. 1994) and  $71.3 \pm 1.6$  Ma (SHRIMP,  $2\sigma$ ) (Nakajima et al. 1993) and intrudes the Inagawa Granite and the Gero Ash-Flow Sheet. The terrestrial Toki Sand and Gravel Beds are of Upper Miocene to Lower Pleistocene age (Editorial Committee of CHUBU II 1988).

The Ueno Basaltic Rocks are extrusive volcano rocks above the Toki Sand and Gravel Bed. K–Ar ages of the Ueno Basaltic Rocks at Sakashita range from  $1.41 \pm 0.12$  Ma (Uto and Yamada 1985),  $1.68 \pm 0.11$  Ma (Shimizu et al. 1988),  $1.64 \pm 0.08$  Ma to  $1.54 \pm 0.08$  Ma (Ujike et al. 1992) with an overall average of  $1.57 \pm 0.05$  Ma ( $2\sigma$ ) based on error propagation indicating a Late Pliocene to Early Pleistocene origin.

The Atera fault in the Kawaue area is separated by the welded tuff of the Gero Ash-Flow Sheet from the Naegi–Agematsu Granite (Fig. 2a, b). The petrography of the welded tuff is described in detail by Niwa et al. (2009) highlighting rhyolitic and phenocryst-rich material, with phenocrysts of quartz, plagioclase, K-feldspar, and biotite in a glassy groundmass supplemented by fine-grained chlorite and quartz. The feldspars remnants are often sericitized. Groundmass alteration results in clay minerals and calcite formation as secondary minerals. The Naegi–Agematsu Granite petrography highlights quartz, plagioclase, K-feldspar mineral phases, and biotite which is partially chloritized and fine-grained (Niwa et al. 2009; 2015).

The Atera Fault outcrops consist of an ~42-m-wide fault zone, divided into numerous damage zones derived from welded tuff and granite, and a narrow 1.2-m-fault core (Fig. 2).

In the western part of the fault zone the dominant welded tuff damage zone is composed of a 10-m-wide zone of welded tuff and a 14-m-wide fault breccia. In the eastern part of the Atera Fault the granite contains a ~1.2-m-wide damage zone and a 5-m-wide granite cataclasite zone. The 1.2-m-wide fault core is clay-rich and contains fragments of welded tuff, granite, and basalt. According to Niwa et al. (2009) remaining basalt fragments correlate with the neighboring volcanic rocks of the Ueno Basaltic Rocks allowing to constraint on the maximum age of fault core formation. The fault core trends NW–SE to NNW–SSE with a subvertical dip. A sinistral sense of shear can be constrained as several rounded fragments have been rotated displaying asymmetric tails. These structural features of the fault core are consistent with the general structure of the Atera Fault (Niwa et al. 2009; 2015). In addition to the 1.2-m-wide fault core, a 30-cm-wide fault overprints the granite cataclasite (Fig. 2c). The fault gouge is clay-rich and includes granite fragments. The trend of the gouge is subparallel to the 1.2-m-wide fault core with NW–SE to NNW–SSE strike, and a subvertical dip and slickenlines on the gouge plunge gently south (Niwa et al. 2015).

## Analytical methods

### Sampling

Three clay-rich gouge samples were obtained from the main outcrop shown in Fig. 2c and selected based on the host rock mineralogy. An undeformed host rock sample of the welded tuff from the Gero Ash-Flow Sheet of the Nohi Rhyolite was collected about 3 km to the west (Tsu-kechi River 1) (Fig. 1c). Sample Atera 1 (3369) originates from the welded tuff fault breccia, sample Atera 2 (3370) from the center of the 1.2-m-wide fault core and sample Kawaue 1 (3367) from the 30-cm-wide fault gouge within the granite cataclasite. The location of the outcrop is shown in Fig. 1c, and GPS location data summarized in Table 1. The procedures applied in this study are based on Zwingmann et al. (2010a, 2011).

About 50 to 100 g of fresh gouge and cataclasite material was collected from each sample site. Sample disintegration involved a gentle repetitive freezing and heating technique which avoids artificial reduction of K-bearing minerals rock components (micas or K-feldspars, see Liewig et al. 1987; Zwingmann et al. 2017). Separated grain-size fractions comprise <2, 2–6 and 6–10  $\mu\text{m}$  obtained according to Stokes' law. Fine grained <0.1  $\mu\text{m}$  fractions were separated using a high-speed centrifuge, but only limited amount could be obtained. For whole-rock host rock analysis a small amount of the sample rock was crushed gently by hand in an agate mortar. Mineralogical characterization of the sample fractions involved

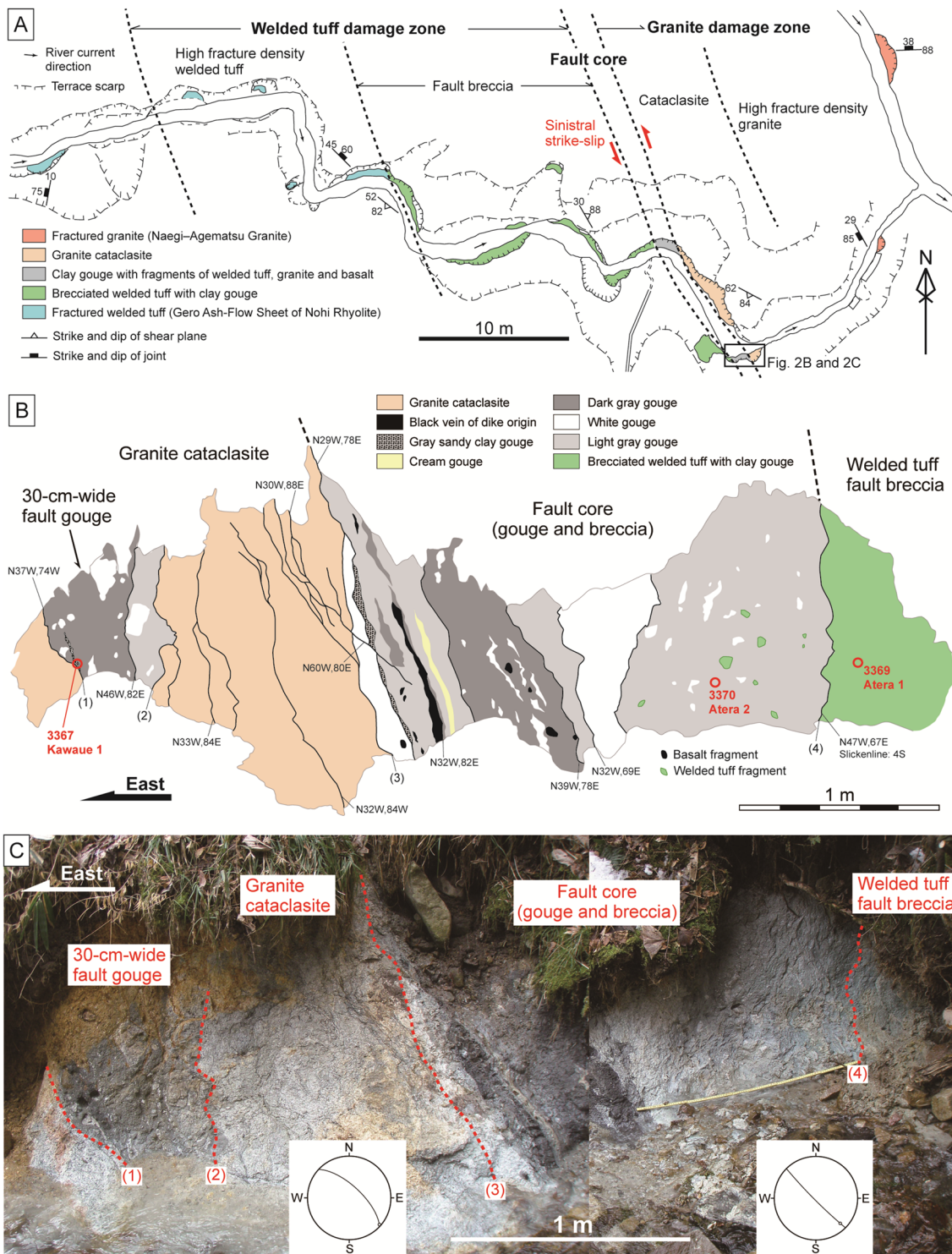


**Fig. 2** Outcrop details. **A** Atera Fault overview Kawaue area, **B**, studied outcrop sketch, **C** outcrop image and structural context of **B** (modified from Niwa et al. 2015). (1) to (4) in **B** and **C** show major lithological boundaries and correspond to each other

**Table 1** GPS outcrop location

Fault gouges:	N35°36′21″ / E137°29′49″
Host rock:	N35°35′58″ / E137°27′51″

X-ray diffraction (XRD), scanning electron microscopy (SEM), and transmission electron microscopy (TEM).

### XRD

The mineralogy of the size fractions was determined by XRD on randomly oriented powder samples. Results for the <0.1  $\mu\text{m}$  fractions could not be obtained due to very limited sample amount and these fractions were mainly investigated by TEM (see below). Diffractograms of the samples were obtained and analyzed using a Rigaku Ultima IV with a two-axis goniometer,  $\text{CuK}\alpha$  radiation, a  $\text{K}\beta$  filter, and a one-dimensional X-ray detector (D/teX Ultra), 40 kV, 30 mA, 0.5° and 10 mm divergence slits, and 8 mm anti-scattering slit. The samples were scanned over the range  $2\theta = 3\text{--}70^\circ$  with a scan rate of  $1^\circ \text{min}^{-1}$  and a step size of  $0.01^\circ$ . The XRD results are listed in Table 2.

### Petrography

The Atera 1 and 2 fault gouge and the host rock samples were investigated by thin section petrography. Petrographic information for sample Kawau 1 (3367) from the 30-cm-wide fault gouge within the granite cataclasite can be found in Niwa et al. (2009).

A low-viscosity epoxy (Struers Epofix) was applied to the fault rock samples before cutting. As the fault rocks might contain clay minerals with different water content, synthetic hydrocarbon oil (ENEOS METAL WORK S) was used during thin section preparation, cutting and grinding. To mount fault sample chips to glass slides Petropoxy 154 was used and mounted sections reduced to  $\sim 35 \mu\text{m}$  thickness and polished. Freshly broken surfaces of sample chips were carbon-coated and examined by SEM in secondary electron mode using a HITACHI TD-1000 SEM equipped with an energy dispersive system

X-ray analyzer (EDS; Horiba EMAX) at the JAEA Tono Geoscience Center, Japan. A JEOL F200 (CF-HR) TEM operating at 200 kV equipped with a Gatan OneView camera was used for comprehensive, grain-by-grain morphological characterization of selected <0.1  $\mu\text{m}$  clay fractions, and to investigate the grain-size distribution at the CMCA, UWA, Perth, Australia. For TEM investigation, samples were prepared by placing one drop of clay solution on a Cu TEM grid with a thin, amorphous carbon support film and drying in air. The composition of individual particles was investigated with a JEOL SD100WL 100 mm<sup>2</sup> SDD (Silicon Drift Detector) EDS detector run through Oxford Instruments' AZtec software.

### K–Ar dating

K–Ar dating follows standard methods given in detail by Dalrymple and Lanphere (1969) and carried out at CSIRO Energy, Perth, Australia, using a procedure similar to that described by Bonhomme et al. (1975). Potassium content was measured by ICP-OES (Agilent Technologies 725 ICP-OES) on  $\sim 20$  mg of sample which was dissolved using HF and  $\text{HNO}_3$  and diluted to 10–50 ppm K. The pooled error of K determination of all samples and standards is better than 2%.

For argon analyses the mineral fraction were fused within a vacuum line connected to a  $^{38}\text{Ar}$  spike pipette. An online VG3600 mass spectrometer was used to measure the isotopic composition of the spiked Ar. The  $^{38}\text{Ar}$  was calibrated against standard biotite GA1550 (McDougall and Roksandic 1974). Special care was taken in the preparation of both K and Ar sample splits as clays are hygroscopic. For Argon analysis the sample splits were loaded into clean Mo-foil (Goodfellow molybdenum foil, thickness 0.025 mm, purity 99.9%), weighed and preheated to  $80^\circ\text{C}$  for 8 h to remove moisture, and re-weighed using a Mettler AT20 balance and the measured dry weight used in the K–Ar age calculation. A desiccator was used for sample storage prior to loading to the argon sample holder. The mass discrimination factor was

**Table 2** XRD data

Sample	ID #	Fraction ( $\mu\text{m}$ )	Smectite (%)	Illite (%)	Chlorite (%)	Quartz (%)	Plagioclase (%)	K-feldspar (%)
Atera 1	3369	<2	44	27	-	10	14	5
		2–6	22	20	-	21	31	6
		6–10	13	12	-	31	35	8
Atera 2	3370	<2	57	30	-	5	5	3
		2–6	43	17	-	18	18	4
Kawau 1	3367	<2	9	33	-	20	28	11
Tsukechi River 1	3510	WR	-	-	6	39	51	5

Semi-quantification based on integrated intensity ratio using reference of corundum, WR whole rock

determined periodically by “airshots” which are small amounts of air for  $^{40}\text{Ar}/^{36}\text{Ar}$  ratio measurements. Blanks were systematically determined for the extraction line and mass spectrometer. Five international standards (3 HD-B1, 2 LP-6) and 4 airshots were analyzed during the course of the study (Table 3). The  $^{40}\text{Ar}/^{36}\text{Ar}$  values of the airshot yielded  $295.63 \pm 0.21$  ( $1\sigma$ ). The error for argon analyses is below 1.0% ( $2\sigma$ ) based on the long-term precision of measurements of international Argon standards. The  $^{40}\text{K}$  abundance and decay constants recommended by Steiger and Jäger (1977) were used for K–Ar age calculation. The age uncertainties consider the errors during sample weighing,  $^{38}\text{Ar}/^{36}\text{Ar}$  and  $^{40}\text{Ar}/^{38}\text{Ar}$  measurements, and K analysis. Ages are reported to the time-scale of Cohen et al. (2013).

## Results

### XRD

The fault clay gouge mineralogy was obtained by XRD analysis. The representative XRD spectra of the  $<2\ \mu\text{m}$  fractions and the host rock powder are summarized in Fig. 3. The fault gouge samples comprise: smectite, illite, quartz, K-feldspar and plagioclase (Table 2). Amounts of smectite and illite increase with decreasing particle size and amounts of quartz, K-feldspar and plagioclase decrease with decreasing particle size. For sample Atera 1, the  $<2\ \mu\text{m}$  fraction contains the highest amount of illite with 27%, decreasing to 20% in the 2–6  $\mu\text{m}$  and 12% in the coarsest 6–10  $\mu\text{m}$  fraction. This trend is similar for the Atera 2 sample with illite enriched in the  $<2\ \mu\text{m}$  fraction with 30% decreasing to 17% in the 2–6  $\mu\text{m}$  fraction. The smectite content of both samples is decreasing in a similar manner for both fault gouge samples from 44% in the  $<2\ \mu\text{m}$  fraction, 22% in the 2–6  $\mu\text{m}$  fraction to 13% in the coarse 6–10  $\mu\text{m}$  fraction for Atera 1 and, 57% for

the  $<2\ \mu\text{m}$  fraction to 43% in the 2–6  $\mu\text{m}$  fraction for the Atera 2 sample, respectively. In both samples the K-feldspar content increases with grain size from 5 to 8% for Atera 1 fractions whereas, for the Atera 2 fractions, K-feldspar content is homogenous  $\sim 3$  to 4%. The Kawau 1 sample contains a high amount of illite at 33%, a low amount of smectite at 9% and a significant K-feldspar content of 11%. The Nohi Rhyolite host rock is rich in quartz, plagioclase, K-feldspar, and chlorite with no illite present. Illite polytype analysis results are inconclusive due to low amounts of sample and mixture of illite and feldspar in the  $<2\ \mu\text{m}$  and coarser fractions.

## Petrography

### Optical microscope petrography

Optical microscopic observation confirms that all Atera Fault gouge samples are clay-rich with distinct foliation and a preferred alignment of minerals (Fig. 4). The Atera 1 sample shows significant development of microfractures in lithic fragments of welded tuff and mineral fragments of quartz and feldspar. Clay minerals are unevenly distributed and concentrated in larger fractures confirming previous studies by Niwa et al. (2009).

The Atera 2 sample originates from the main fault core and contains polymineralic fragments of welded tuff, granite, and andesite/basalt, and monomineralic fragments of quartz, plagioclase, and K-feldspar in a clay matrix. The fragments are subangular to subrounded. Fine fragments of well aligned phyllosilicates and quartz are observed in the clay matrix. Additional petrographic information of the Atera Fault zone can be found in Niwa et al. (2009).

Contrary to the Atera fault samples, the thin section petrography of the Nohi Rhyolite host rock indicates no

**Table 3** K–Ar standards and airshot data

CSIRO ID Standard	K (%)	Rad. $^{40}\text{Ar}$ (mol/g)	Rad. $^{40}\text{Ar}$ (%)	Age* (Ma)	Error (Ma)	Remark % error to references
HD-B1-154	7.96	3.4055E-10	92.16	24.51	0.33	1.24
HD-B1-157	7.96	3.3524E-10	90.12	24.13	0.32	-0.33
HD-B1-156	7.96	3.4037E-10	91.30	24.50	1.38	1.20
LP6-171	8.37	1.9222E-09	97.12	127.77	1.64	-0.10
LP6-170	8.37	1.9144E-09	97.00	127.27	1.31	-0.49
Airshot ID			$^{40}\text{Ar}/^{36}\text{Ar}$			$\pm$
AS148-AirS-2			295.95			0.18
AS148-AirS-2			295.74			0.22
AS150-AirS-1			295.41			0.27
AS151-AirS-2			295.40			0.16

References HD-B1 (Hess and Lippolt 1994), LP6 (Odin et al., 1982), airshot (Steiger and Jäger 1977)

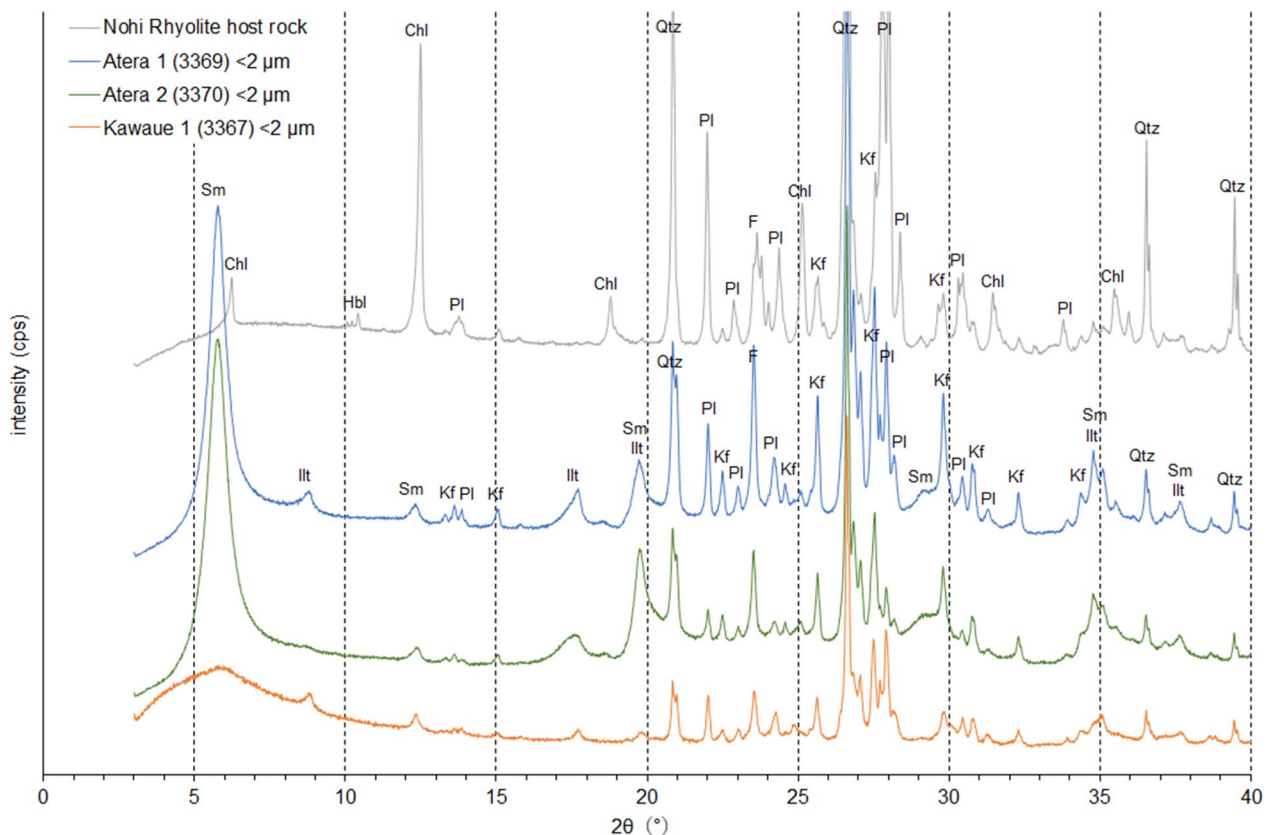


**Fig. 3** Representative XRD spectra showing the <2  $\mu\text{m}$  fractions and the host rock sample. Sm: smectite, Illt: illite, Qtz: quartz, F: feldspar, Kf: K-feldspar, Pl: plagioclase, Chl: chlorite, Hbl: hornblende

foliation and few microfractures. The host rock sample contains large ~1–3 mm quartz and plagioclase minerals as well as chloritized mafic minerals. The fine-grained groundmass is mainly composed of quartz and plagioclase. The quartz phenocrysts are often corroded and plagioclase mostly sericitized.

### SEM results

SEM investigations reveal that smectite/illite minerals in the fault gouge zones document preferred orientation and exhibit well crystallized euhedral grain boundaries, related to an authigenic and synkinematic origin, compared to host rock samples as shown in Fig. 5 (Clauer and Chaudhuri 1995). However, no direct anastomosing foliation defined by illite/smectite (I/S) coatings around clasts of host rock can be observed. The observed gouge minerals are interpreted to be of synkinematic origin due to the preferred orientation. Irregular remaining host rock grains are surrounded by a finer grained matrix and might be a result of mechanical comminution in contrast to forms more typical of well-crystallized, authigenic clay minerals comprising fibrous, lath-shaped or platelet morphologies (Inoue et al. 1988; Pevear 1999). The

petrographic observations are similar to a study focusing on retrograde faults from the Swiss Alps (Mancktelow et al. 2015). Features revealed by the SEM are different from the fault gouge and Nohi Rhyolite host rock. Euhedral mineral grains mostly composed of quartz and feldspar are filled tightly, without fragmentation. The SEM observed and investigated particles comprise: Al, Si, O, K and Fe as determined by EDS, and correspond to smectite/illite minerals as identified by XRD.

### TEM results

TEM investigations of the selected <0.1  $\mu\text{m}$  clay fractions indicate distinct idiomorphic platy illite flakes, with well crystallized euhedral edges (Fig. 6), and minor electron dense dark particles with diffuse and irregular edges often interpreted as detrital in origin (Clauer and Chaudhuri 1995) (Fig. 6). The particles investigated by TEM EDS contain mainly: Al, Si, O, K and Fe and correspond to smectite/illite minerals as confirmed by SEM and XRD. Detrital clay particles are often volumetrically larger than neoformed illite particles and are characterized by different morphological shapes and often exhibit irregular edges, while neoformed illite particles



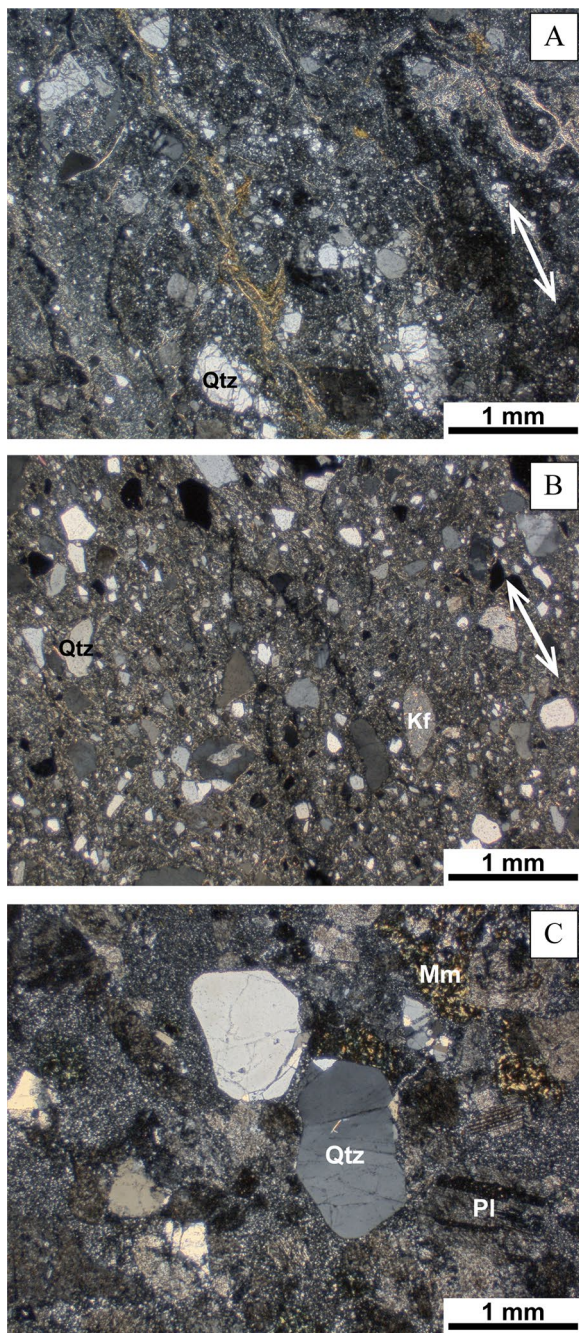


**Fig. 4** Thin section petrography (crossed polarized light). Foliation is developed in the fault rock samples of A. Atera 1 and B. Atera 2 (white arrows), C. host rock. Qtz: quartz, Kf: K-feldspar, Pl: plagioclase, Mm: chloritized mafic mineral

have sharp, well-defined edges (Clauer and Chaudhuri 1995). The idiomorphic platy shapes and morphology of the fault gouge illite particles highlighted by TEM confirms an in situ neof ormation.

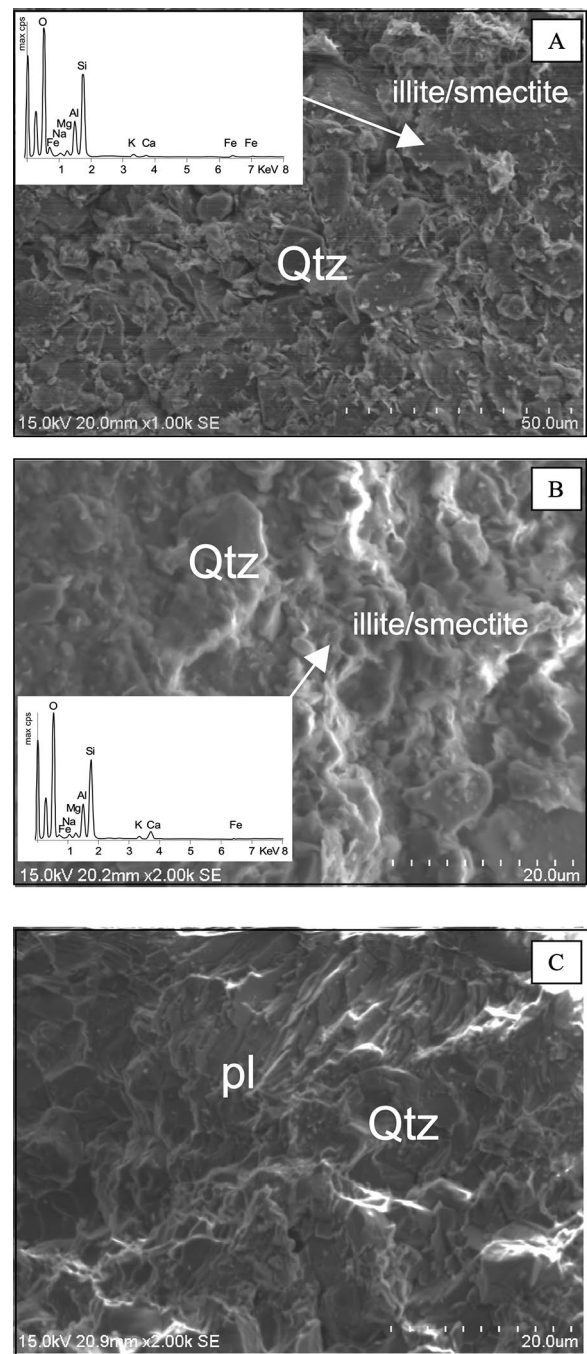


**Fig. 5** SEM images with EDS results showing illite/smectite. Qtz: quartz, Pl: plagioclase. A. Atera 1 Fault gouge, B. Atera 2 Fault gouge, C. host rock

#### K–Ar data

Nine new K–Ar analyses covering one whole rock sample and eight clay fractions from <0.1 to 6–10 μm, were obtained in this study (Table 4). The whole rock analysis

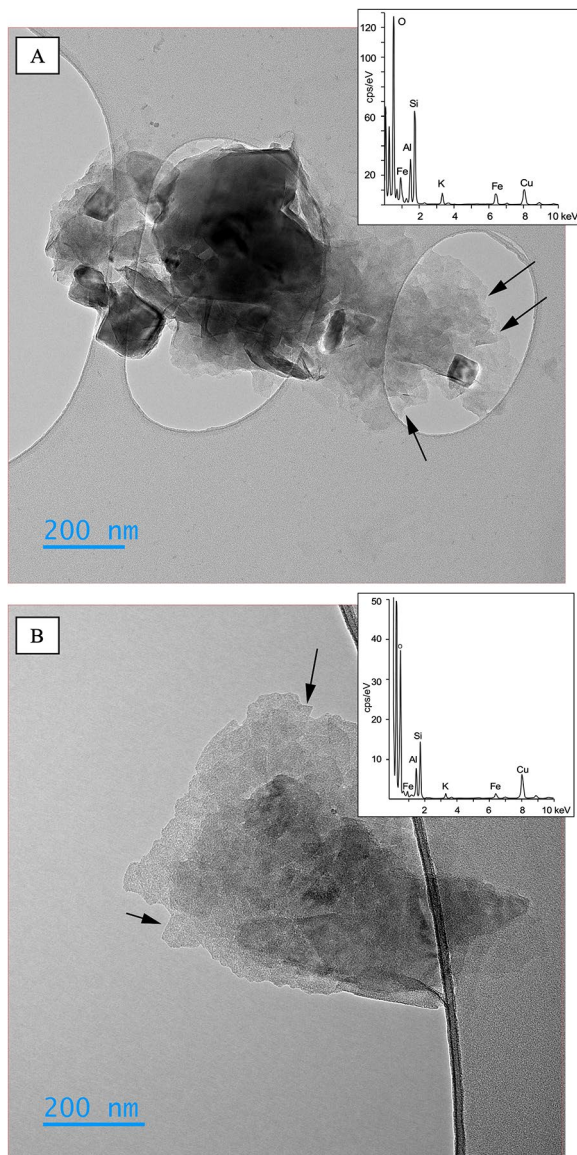


**Fig. 6** TEM images with EDS results showing illite/smectite particles (arrows). A. Atera 1 <0.1  $\mu\text{m}$ , B. Atera 2 <2  $\mu\text{m}$

of an undeformed host rock yields an age of  $54.9 \pm 1.3$  Ma (Paleogene–Eocene–Ypresian) and the Atera fault gouge clay ages range from 40.6 to 60.0 Ma (Paleogene–Eocene–Bartonian to Paleogene–Paleocene–Selandian). As reported in numerous studies involving clay-size fractions, a consistent decrease in age with decreasing grain size can be observed (Fig. 7) (see summaries in Vrolijk et al. 2018; Tsukamoto et al. 2020). The ages of the <2  $\mu\text{m}$  fractions from the three fault gouge samples vary significantly: from  $50.2 \pm 1.2$  Ma for Atera 1, to  $47.0 \pm 1.1$  Ma for Kawau 1 and  $44.1 \pm 1.0$  Ma for sample Atera 2. Ages of the Atera 1 sample originating within the welded tuff

breccia range from  $40.6 \pm 1.0$  Ma for the finest <0.1  $\mu\text{m}$  fraction to  $60.0 \pm 1.4$  Ma for the coarsest 6–10  $\mu\text{m}$  fraction. Ages of the Atera 2 samples originating from the fault gouge yield an age of  $41.8 \pm 1.0$  Ma for the finest <0.1  $\mu\text{m}$  fraction (identical within error of the Atera 1 <0.1  $\mu\text{m}$  sample) and a significantly younger age of  $52.7 \pm 1.2$  Ma for the coarser 2–6  $\mu\text{m}$  fraction. K concentration ranges from 2.74 to 4.98% and radiogenic  $^{40}\text{Ar}$  content from 78.9 to 95.7% indicating no significant contamination with atmospheric  $^{40}\text{Ar}$ .

## Discussion

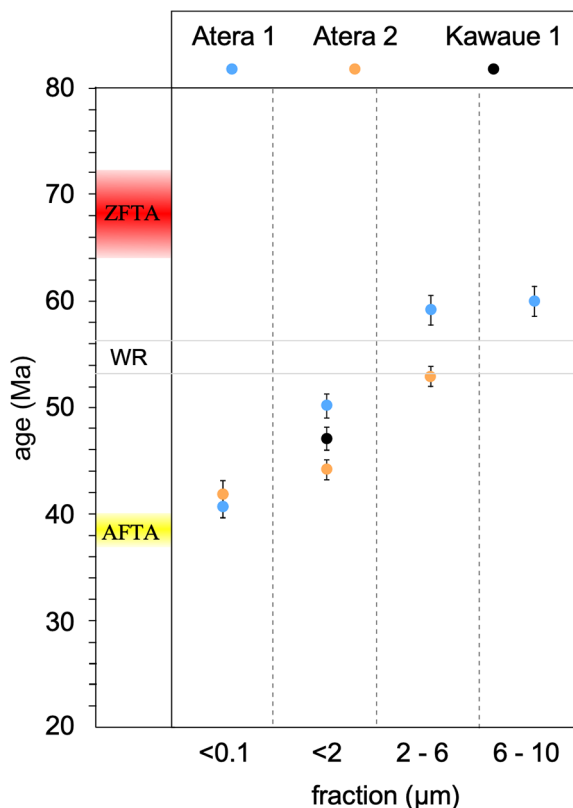
K–Ar dating of authigenic clays and illite in general, including fault gouge, requires careful investigations as discussed by Clauer et al. (2012) and Meunier and Velde (2004). The potential and limitations of K–Ar illite fault gouge dating is discussed elsewhere (see Vrolijk et al. 2018; Tsukamoto et al. 2020). The grain-size fractions of the separated authigenic illite are mixtures of illite particles formed at different times during growth and the formation history is normally investigated by dating a range of different grain-size fractions. Fault gouge illite forms in low-temperature retrograde environments governed by kinetic processes compared to equilibrium thermodynamics of mineral formation processes (e.g., Vrolijk and van der Pluijm 1999; Zwingmann and Mancktelow 2004). We interpret the obtained ages as maximum ages as the authigenic illite within the finest separated particle size represents the most recently grown illite.

Increasing K–Ar ages with increasing grain size are illustrated in Figs. 7 and 8 and related to increased contamination in the coarse fractions compared to the finer fractions as confirmed by XRD data (Table 2). The Atera 1 gouge sample originates from a heterogeneous welded tuff breccia zone and the finest <0.1  $\mu\text{m}$  fraction yields an age of  $40.6 \pm 1.0$  Ma and increases significantly by  $\sim 10$  Ma to  $50.2 \pm 1.2$  Ma for the coarser <2  $\mu\text{m}$  fraction. For the coarser, 2–6  $\mu\text{m}$  and 6–10  $\mu\text{m}$  fraction, the ages increase again by a steep 10 Ma to  $59.1 \pm 1.4$  Ma and  $60.0 \pm 1.4$  Ma, respectively. A similar but less severe age increase is observed for the Atera 2 gouge sample originating from the fault core with the finest <0.1  $\mu\text{m}$  fraction yielding an age of  $41.8 \pm 1.0$  Ma increasing by about 2 Ma to  $44.1 \pm 1.0$  Ma for the coarser <2  $\mu\text{m}$  fraction. The age increases again by a significant 10 Ma to  $52.7 \pm 1.2$  Ma for the coarser 2–6  $\mu\text{m}$  fraction compared to the <0.1  $\mu\text{m}$  fraction. For the Kawau 1 gouge sample (3367) obtained from within the granite cataclasite zone, only a <2  $\mu\text{m}$  fraction was analyzed which yielded an age of  $47.0 \pm 1.1$  Ma. This age is intermediate between the Atera 1 and 2, <2  $\mu\text{m}$  ages. The obtained whole rock host rock age is similar to the coarser 2–6 and 6–10  $\mu\text{m}$  fractions from the fault zone samples (Fig. 7) and suggesting

**Table 4** K–Ar age data

Sample	Type	ID	K (%)	Rad. <sup>40</sup> Ar (mol/g)	Rad. <sup>40</sup> Ar (%)	Age (Ma)	Error (Ma)	Timescale
								Period–epoch–stage
Atera 1	Welded tuff breccia	3369 <0.1	3.56	2.5354E-10	78.9	40.6	1.0	Paleogene–Eocene–Bartonian
		3369 <2	4.44	3.9201E-10	93.7	50.2	1.2	Paleogene–Eocene–Ypresian
		3369 2–6	4.00	4.1703E-10	94.9	59.1	1.4	Paleogene–Paleocene–Thanetian
		3369 6–10	3.92	4.1464E-10	95.7	60.0	1.4	Paleogene–Paleocene–Selandian
Atera 2	Fault core	3370 <0.1	2.74	2.0091E-10	89.5	41.8	1.0	Paleogene–Eocene–Lutetian
		3370 <2	2.80	2.1694E-10	88.3	44.1	1.0	Paleogene–Eocene–Lutetian
		3370 2–6	3.18	2.9515E-10	92.6	52.7	1.2	Paleogene–Eocene–Ypresian
Kawaue 1	Granite cataclasite	3367 <2	4.98	4.1180E-10	92.9	47.1	1.1	Paleogene–Eocene–Lutetian
Tsukechi River 1	Welded tuff host rock	3510 WR	1.57	1.5170E-10	81.6	54.9	1.3	Paleogene–Eocene–Ypresian

WR whole rock, timescale Cohen et al. (2013)

**Fig. 7** K–Ar age versus grain-size plot. AFTA apatite fission-track ages, ZFTA zircon fission-track ages, WR whole rock

a thermal overprint or hydrothermal overprint might be associated with the fault initiation around 41.2 Ma and, might have partially influenced and reset the isotopic signatures of the Nohi Rhyolite host rock. The K–Ar ages of <2 μm fractions from the Atera fault gouges from our study fall within the age range reported by Yamada et al. (1992), ranging from 38 to 55 Ma. Yamada et al. (1992)

only reported a limited <2 μm fraction age data without detailed description of the investigated fault rocks, whereas this study includes detailed gouge K–Ar age data from different size fractions including finer, <0.1 μm fractions in a well-described fault zone outcrop of the Atera Fault.

The increase in ages of both fault gouge samples can be explained by increasing K-feldspar contamination (Table 2) and highlights that the most reliable isotopic ages for authigenic illite can be obtained from the finest size fractions (<0.1 μm or finer) of gouge rock samples due to minimal contamination as discussed by Zwingmann et al. (2010a, 2011), Torgersen et al. (2015) and Viola et al. (2016). The average age of the two <0.1 μm Atera gouge fractions yields a mean of  $41.2 \pm 0.7$  Ma, which is significantly younger than the <2 μm fraction ages of  $47.2 \pm 0.8$  Ma, and correspond, within error, to the age obtained from the gouge sample within the granite cataclasite zone (Kawaue 1, 3367). The ages of all size fractions are relatively heterogenous suggesting that: (1) different contamination sources might be present in the fault gouge samples, or (2) the fault core sample experienced a more severe last faulting event suggesting an increasing effect of mechanical comminution toward the fault core (Fukuchi et al. 2014).

### Implications for geology of Central Japan

As discussed by Zwingmann and Mancktelow (2004, Zwingmann et al. (2010a; 2010b) and Yamasaki et al. (2013) the K–Ar ages of fault gouge illite are bracketed by the zircon and apatite fission-track ages from host rocks (Fig. 8). Authigenic illite formation during brittle deformation is closely related to temperature ranges and occurs between the partial annealing zones of apatite, ranging from a low 60–120 °C (see references in Yamasaki et al. 2013), to a higher 170–390 °C range for zircon

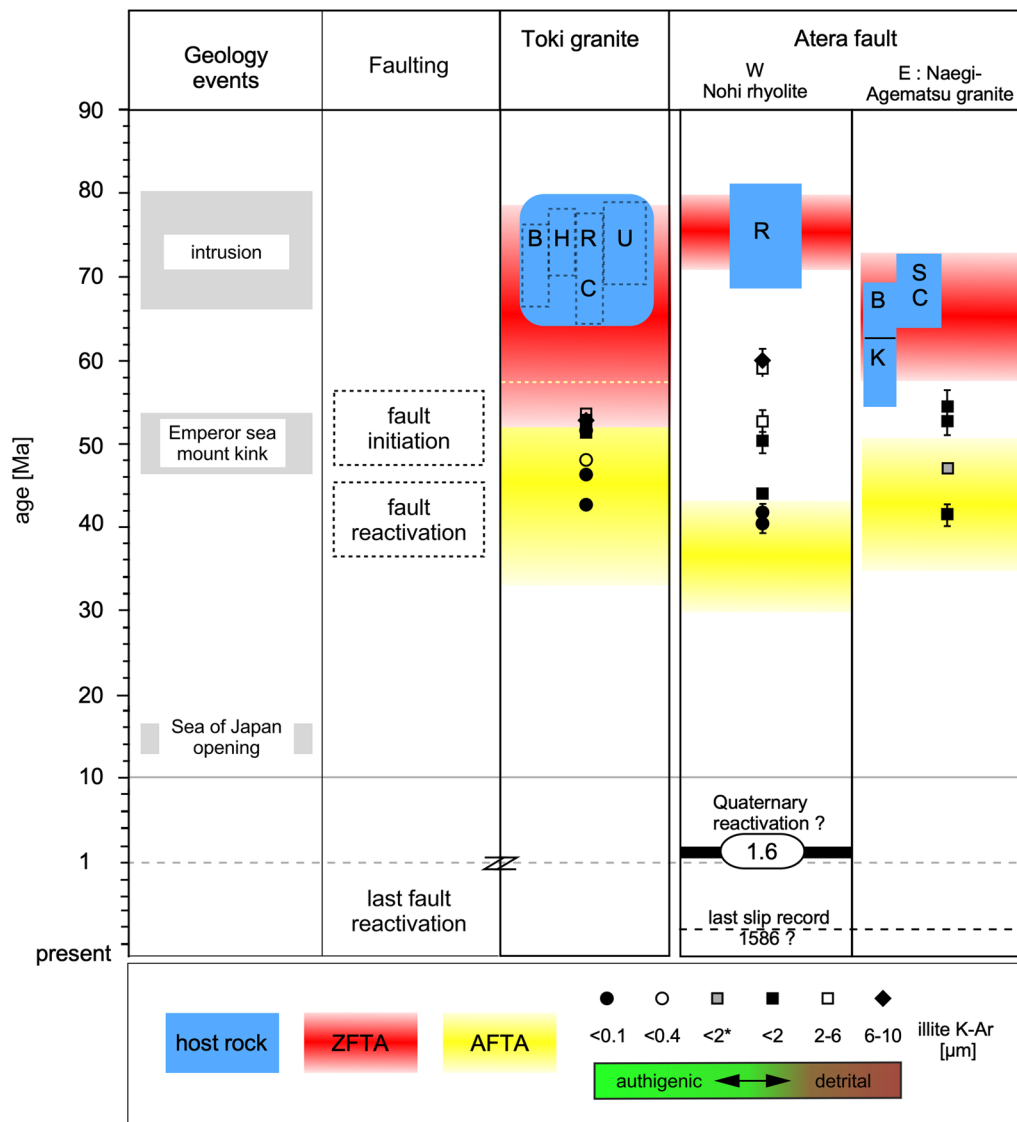


**Fig. 8** K–Ar age data in the geochronological context of the study area in Central Japan. Toki Granite host rock data based on Shibara and Ishihara (1979), Suzuki and Adachi (1998), Yamasaki and Umeda (2012), Yuguchi et al. (2019) and Yamasaki et al. (2013). B biotite, H hornblende, R Rb–Sr, C Chime (chemical U–Th total Pb isochron method), U U–Pb, K K-feldspar, S Shrimp U–Pb. Opening of Japan sea based on Hoshi et al. (2015)

(Yamada et al. 1995). Similar to the limited brittle fault illite age data from the Toki Granite (Yamasaki et al. 2013), the age of main illite formation within the Atera Fault of ~47.1 Ma is younger than the reported fault gouge illite age data from the Nojima Fault ca. 250 km to the SW (Zwingmann et al. 2010b).

However, numerous Paleogene–Early Eocene illite fault gouge ages are reported in Japan along the Median Tectonic Line in the Shikoku and Kinki area about 200–350 km to the SW and the Mozumi–Sukenobu Fault about 100 km to the N (e.g., Yamasaki et al. 2013). The active faults are related to the Cretaceous granite margin and

Jurassic accretionary complexes in the Inner Zone of SW Japan (Takagi et al. 2005). As discussed by Yamasaki et al. (2013) significant hydrothermal events accompany faults in SW Japan, ranging in age from ca. 60–50 Ma. Subsequent to clay formation hydrothermal fluid circulation is limited to the fault core and thus unable to form new clay minerals during fault reactivation. In our study, the age difference between the Nohi Rhyolite breccia zone sample (Atera 1), and the fault core sample (Atera 2), might indicate a later reactivation. This is similar to gouge samples in other case studies comprising the Deokpori Thrust, Korea, and the Nojima Fault, Japan, suggesting

age variation with decreasing ages in grain size is caused by potential fault reactivation (Zwingmann et al. 2010b, 2011). Illite age data reported by Yamasaki et al. (2013) for the nearby Toki Granite suggest that brittle faults were influenced by a later thermal event within the illite formation, the temperature ranging between 80 and 200 °C (see Zwingmann et al. 2019) yielding ages around 54 to 43 Ma and no illite ages related to an earlier 43 Ma (Paleogene–Middle Eocene) hydrothermal fluid event.

The thermochronological history and cooling curve of the study area for the nearby Toki Granite was summarized by Yamasaki et al. (2013) (Fig. 9A) and we adapted and approximated the thermochronological history and well-defined cooling curve for the Nohi Rhyolite and Naegi–Agematsu Granite (Fig. 9B). Ages are plotted from high closing to low closing temperature of minerals based on Yamada et al. (1992), Nakajima et al. (1993), Suzuki et al. (1994), Shirahase (2005), and Yamada et al. (2012). The age data of monazite CHIME, whole rock Rb–Sr, hornblende, biotite K–Ar, and ZFTA for host rocks from the Nohi Rhyolite and Naegi–Agematsu Granite are similar to the nearby Toki Granite.

The summarized complex thermochronological data support a model from Yamasaki et al. (2013), with a pluton intrusion at ~70 Ma and subsequent rapid cooling to ~300 °C. As outlined for the Toki Granite setting, the Naegi–Agematsu Granite experienced a similar rapid cooling after intrusion followed by slow cooling

and associated with successive exhumation between the ZFTA and AFTA closure temperatures of zircon (~300°C) and apatite (~100°C), respectively, at a cooling rate of ~7–9°C/m.y. as suggested by Yamasaki and Umeda (2012).

The newly obtained K–Ar illite ages ranging from 40 to 60 Ma for the Atera 1 sample fraction and 41 to 53 Ma for Atera 2 fractions, plot on the 100–200°C temperature range of this cooling curve similar to the Toki Granite fault gouge formation (Fig. 9A). The <0.1 μm fractions of both Atera fault gouge samples yield ages identical within error around 40 Ma, whereas the <2 μm ages vary by 5 Ma from 50 to 44 Ma which might be caused by variable K-feldspar contamination. As the Kawaue 1 <2 μm fraction contains the highest amount of K-feldspar contamination of ~11% but yields an intermediate age of 47 Ma, the overall impact of contamination might be negligible as the K-feldspar might be partially reset (Zwingmann et al. 2010a). The new Atera Fault gouge illite age data confirm that brittle deformation and thermal events are synchronous with the post-intrusive uplifting in this part of Central Japan (Yamasaki et al. 2013). The Atera Fault illite age data might provide new insights into an integrated regional-scale record of tectonic displacement in Central Japan and might be influenced by large-scale tectonic processes such as the Emperor sea mount kink around 50 to 46 Ma (Torsvik et al. 2017; Kubota et al. 2020) with fault initiation around 55 Ma

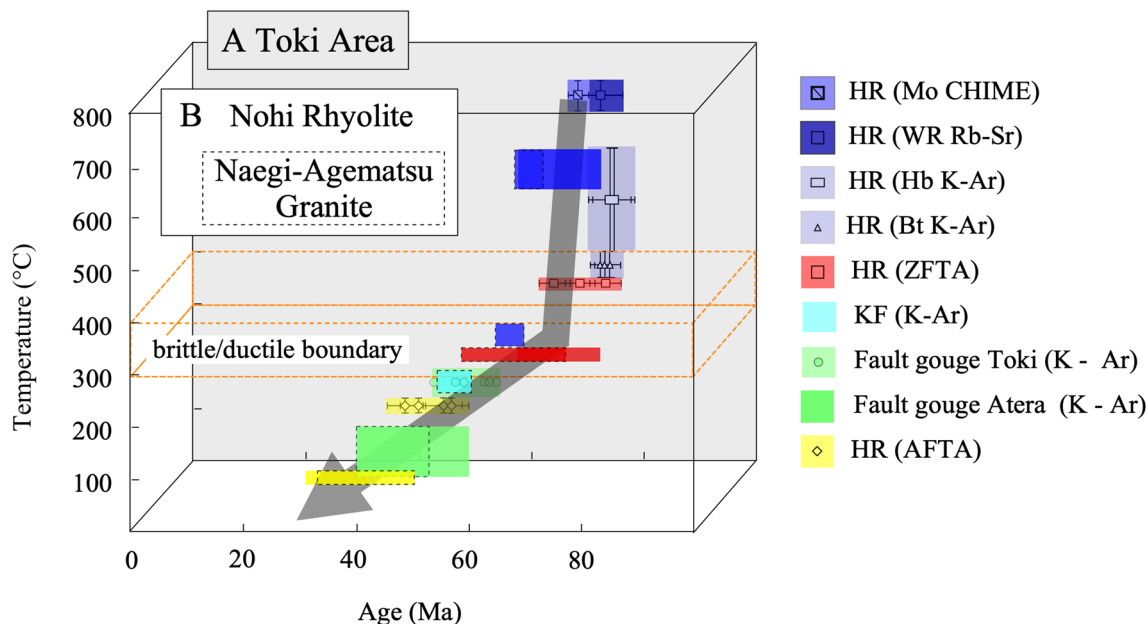


**Fig. 9** Thermochronological summary of study area. A. Toki area (background grey shade) based on Yamasaki et al. (2013), opaque square, rectangle, triangle and circle symbols indicate Toki area thermochronology data. B. Nohi Rhyolite and Naegi–Agematsu Granite area (front), cooling curve modified from Yamasaki et al. (2013). HR host rock, Hb hornblende, Bt biotite, KF K-feldspar, Mo monazite CHIME chemical U–Th total Pb isochron method, WR whole rock

and brittle fault cessation or reactivation around 40 Ma in the Eocene. Recent geodynamic modeling by Hu et al. (2022) provides an additional insight into the geotectonic dynamics caused by an abrupt change in the Pacific Plate movement around 50 Ma and support a Hawaiian–Emperor sea mount kink influence. In addition, Kubota et al. (2020) discuss a potential 46.4–47.0 Ma event for the MTL (Median Tectonic Line) corresponding to the change of direction of the Pacific oceanic plate motion. In addition, similar illite K–Ar ages were reported for Nojima Fault gouges by Zwingmann et al. (2010b).

## Conclusions

Complex fault cores and brittle fault rocks are rarely preserved in outcrops in Japan due to extensive weathering, erosion and/or vegetation cover. River outcrops and fresh exposures therefore provide important opportunities to investigate the fault zones and architecture of regionally important tectonic frameworks. The results presented from the Atera Fault in Central Japan form an internally consistent data set, supported by a large amount of geochronological data (AFTA, ZFTA, CHIME), demonstrating the application of gouge dating and provide new data constraining the timing of brittle deformation in Central Japan. The new illite age data from the well-exposed Atera Fault complete recently obtained, limited fault illite gouge age data from the Toki Granite (Yamasaki et al. 2013), and are, within error, identical. The age of the heterogeneous welded tuff breccia zone (Atera 1) ranges from  $40.6 \pm 1.0$  Ma to  $60.0 \pm 1.4$  Ma (Eocene–Bartonian–Paleocene–Selandian). The age of the fault core gouge sample (Atera 2) ranges from  $41.8 \pm 1.0$  Ma to  $52.7 \pm 1.2$  Ma (Eocene–Lutetian–Ypresian). The finest  $< 0.1 \mu\text{m}$  fraction of the fault breccia and fault core gouge yield within error identical ages of around 41 Ma (Eocene–Bartonian). Similar to the nearby Toki Granite, the data constrain the timing of brittle deformation followed by a geothermal event in the Paleogene–Eocene. Brittle deformation and thermal event are related to the post-intrusive exhumation of Cretaceous granite. The new Atera Fault illite ages are comparable with results reported from other faults in the Inner Zone of SW Japan including the Median Tectonic Line, the Mozumi–Sukenobu Fault and the Nojima Fault (Shibata et al. 1989; Yamada et al. 1992; Zwingmann et al. 2010b) and might be related to large-scale tectonic processes, i.e., Emperor sea mount kink around 50 to 46 Ma (Torsvik et al. 2017; Kubota et al. 2020; Hu et al. 2022).

## Acknowledgements

This study was funded by METI, Japan, as part of its R&D supporting program titled “Establishment of Advanced Technology for Evaluating the Long-term Geosphere Stability on Geological Disposal Project of Radioactive Waste (JPJ007597) (Fiscal Years 2018–2022)”. The authors acknowledge the facilities,

and the scientific and technical assistance of Microscopy Australia at the Centre for Microscopy, Characterization & Analysis, The University of Western Australia, a facility funded by the University, State and Commonwealth Governments. We thank two anonymous reviewers for constructive reviews improving the manuscript.

## Author contributions

The main idea was developed by HZ and NM and all authors contributed to the writing of the text. XRD, SEM and thin section analyses were conducted by NM and HZ. K–Ar geochronology was established by HZ and AT. TEM data were provided by MS in collaboration with HZ. All authors discussed the results and commented on the manuscript.

## Availability of data and materials

All data in this study can be obtained in the figures, tables and references. All data are available at KURENAI, Kyoto University’s institutional repository at <https://doi.org/10.57723/286824>.

## Declarations

### Competing interests

The authors declare no competing interests.

### Author details

<sup>1</sup>Department of Geology and Mineralogy, Kyoto University, Sakyo-Ku, Kyoto 606-8502, Japan. <sup>2</sup>Tono Geoscience Center, Japan Atomic Energy Agency, 959-31, Jorinji, Izumi, Toki 509-5102, Japan. <sup>3</sup>CSIRO Energy, 26 Dick Perry Drive, Kensington, WA 6151, Australia. <sup>4</sup>UWA, Centre for Microscopy, Characterization and Analysis, M010, Perth, WA 6009, Australia.

Received: 13 January 2024 Accepted: 24 January 2024

Published online: 07 February 2024

## References

- Bonhomme MG, Thuizat R, Pinault Y, Clauer N, Wendling R, Winkler R (1975) Methodé de Datation Potassium–Argon: Appareillage et Technique, 53 pp., Cent. de Geochem. de la Surface, Univ. Louis Pasteur, Strasbourg, France
- Clauer N, Chaudhuri S (1995) Clays and Crustal Cycles. Springer, Heidelberg
- Clauer N, Zwingmann H, Liewig N, Wendling R (2012) Comparative  $^{40}\text{Ar}/^{39}\text{Ar}$  and K–Ar dating of illite-type clay minerals: a tentative explanation for age identities and differences. *Earth-Sci Rev* 115:76–96. <https://doi.org/10.1016/j.earscirev.2012.07.003>
- Cohen KM, Finney SC, Gibbard PL, Fan J-X (2013) updated The ICS International Chronostratigraphic Chart. Episodes 36, 199–204. Updated v2019/05 [www.stratigraphy.org/ICSchart/ChronostratChart2019-05.pdf](http://www.stratigraphy.org/ICSchart/ChronostratChart2019-05.pdf)
- Dalrymple GB, Lanphere MA (1969) Potassium–Argon Dating: Principles, Techniques and Applications to Geochronology, 258 pp., W. H. Freeman, San Francisco, Calif.
- Editorial committee of Chubu II, (1988) Regional Geology of Japan Part 5 CHUBU II. Kyoritsu Shuppan Co., Ltd, Tokyo (in Japanese)
- Fukuchi R, Fujimoto K, Kameda J, Hamahashi M, Yamaguchi A, Kimura G, Hamada Y, Hashimoto Y, Kitamura Y, Saito S (2014) Changes in illite crystallinity within an ancient tectonic boundary thrust caused by thermal, mechanical, and hydrothermal effects: an example from the Nobeoka Thrust, southwest Japan. *Earth Planets Space* 66:116. <https://doi.org/10.1186/1880-5981-66-116>
- Heinecke C, Hetzel R, Nilius N-P, Zwingmann H, Todd A, Mulch A, Wölfler A, Glotzbach C, Akal C, Dunkl I, Hampel A (2019) Timing of detachment faulting in a symmetric core complex from K–Ar dating of fault gouge. *J Struct Geol* 127:89. <https://doi.org/10.1016/j.jsg.2019.103865>
- Hess JC, Lippolt HJ (1994) Compilation of K–Ar measurements on HD-B1 standard biotite, in Phanerozoic Time Scale, Bull. Liaison Inf., vol. 12, pp. 19–23, edited by G. S. Odin, IUGS Subcomm. Geochronology, Paris.
- Hetzel R, Zwingmann H, Mulch A, Gessner K, Akal C, Hampel A, GÜngör T, Petschick R, Mikes T, Wedin F (2013) Spatio-temporal evolution of brittle normal faulting and fluid infiltration in detachment fault systems - a

- case study from the Menderes Massif, western Turkey. *Tectonics* 32:1–13. <https://doi.org/10.1002/tect.20031>
- Holdsworth RE, Butler CA, Roberts AM (1997) The recognition of reactivation during continental deformation. *J Geol Soc Lond* 154:73–78
- Hoshi H, Kato D, Ando Y, Nakashima K (2015) Timing of clockwise rotation of Southwest Japan: constraints from new middle Miocene paleomagnetic results. *Earth Planets Space* 67:92. <https://doi.org/10.1186/s40623-015-0266-3>
- Hu J, Gurnis M, Rudi J, Stadler G, Mueller RD (2022) Dynamics of the abrupt change in Pacific Plate motion around 50 million years ago. *Nat Geosci* 15:74–78. <https://doi.org/10.1038/s41561-021-00862-6>
- Inoue A, Velde B, Meunier A, Touchard G (1988) Mechanism of illite formation during smectite-to-illite conversion in a hydrothermal system. *Am Miner* 73:1325–1334
- Kemp SJ, Gillespie MR, Leslie GA, Zwingmann H, Diarmad S, Campbell G (2019) Clay mineral dating of displacement on the Sronlairig Fault: implications for Mesozoic and Cenozoic tectonic evolution in northern Scotland. *Clay Miner* 54:181–196. <https://doi.org/10.1180/clm.2019.25>
- Kubota Y, Takeshita T, Yagi K, Itaya T (2020) Kinematic analyses and radiometric dating of the large-scale paleogene two-phase faulting along the median tectonic line, Southwest Japan. *Tectonics*, 39, e2018TC005372 <https://doi.org/10.1029/2018TC005372>
- Liewig N, Clauer N, Sommer F (1987) Rb–Sr and K–Ar dating of clay diagenesis in Jurassic sandstone oil reservoirs, North Sea. *Am Asso Petrol Geol Bull* 71:1467–1474
- Lynch EA, van der Pluijm B (2016) Meteoric fluid infiltration in the Argentine Precordillera fold-and-thrust belt: Evidence from H isotopic studies of neformed clay minerals. *Lithosphere* 9:134–145. <https://doi.org/10.1130/L568.1>
- Mancktelow N, Zwingmann H, Campani M, Fügenschuh B, Mulch A (2015) Timing and conditions of brittle faulting on the Silltal-Brenner Fault Zone, Eastern Alps (Austria). *Swiss J Geosci* 108:305–326. <https://doi.org/10.1007/s00015-015-0179-y>
- Mancktelow N, Zwingmann H, Mulch A (2016) Dating of fault gouge from the Naxos detachment (Cyclades, Greece). *Tectonics* 35:2334–2344. <https://doi.org/10.1002/2016TC004251>
- McDougall I, Roksandic Z (1974) Total fusion  $^{40}\text{Ar}/^{39}\text{Ar}$  ages using HIFAR reactor. *J Geol Soc Aust* 21:81–89. <https://doi.org/10.1080/00167617408728836>
- Meunier A, Velde B (2004) *Illite: Origins. Evolution and Metamorphism*, Springer, Berlin, p 286
- Middleton AW, Uysal IT, Bryan SE, Hall CM, Golding SD (2014) Integrating  $^{40}\text{Ar}$ – $^{39}\text{Ar}$ ,  $^{87}\text{Rb}$ – $^{87}\text{Sr}$  and  $^{147}\text{Sm}$ – $^{143}\text{Nd}$  geochronology of authigenic illite to evaluate tectonic reactivation in an intraplate setting, central Australia. *Geochim Cosmochim Acta* 134:155–174. <https://doi.org/10.1016/j.gca.2014.02.048>
- Moreno T, Wallis S, Kojima T, Gibbison W (eds) (2016) *The Geology of Japan*. Geological Society, London
- Mottram CM, Kellett D, Baressi T, Zwingmann H, Friend M, Todd A, Percival JB (2020) Syncing fault rock clocks: Direct comparison of U–Pb carbonate and K–Ar illite fault dating methods. *Geology* 48:1179–1183. <https://doi.org/10.1130/G47778.1>
- Nakajima T, Williams IS, Watanabe T (1993) SHRIMP U–Pb ages of the Ryoke and Sanyo granitoids in Southwest Japan. In: Abstract of the 100th Annual Meeting of the Geological Society of Japan, 358. [https://doi.org/10.14863/geosocabst.1993.0\\_584](https://doi.org/10.14863/geosocabst.1993.0_584)
- Niwa M, Mizuochi Y, Tanase A (2009) Reconstructing the evolution of fault zone architecture: Field-based study of the core region of the Atera Fault, Central Japan. *Island Arc* 18:577–598. <https://doi.org/10.1111/j.1440-1738.2009.00674.x>
- Niwa M, Mizuochi Y, Tanase A (2015) Changes in chemical composition caused by water–rock interactions across a strike-slip fault zone: case study of the Atera Fault, Central Japan. *Geofluids* 15:387–409. <https://doi.org/10.1111/gfl.12096>
- Nuriel P, Weinberger R, Kylander-Clark ARC, Hacker BR, Craddock JP (2017) The onset of the Dead Sea transform based on carbonate age-strain analyses. *Geology* 45:587–590. <https://doi.org/10.1130/G38903.1>
- Odin G.S., 35 collaborators (1982) Interlaboratory standards for dating purposes, in *Numerical Dating in Stratigraphy*, vol. 1, edited by G. S. Odin, pp. 123–148, John Wiley, Chichester, U. K.
- Pevear DR (1999) Illite and hydrocarbon exploration. *Proc Natl Acad Sci* 96:3440–3446
- Roberts NMW et al (2020) Laser ablation inductively coupled plasma mass spectrometry (LA–ICP–MS) U–Pb carbonate geochronology: Strategies, progress, and limitations. *Geochronology* 2:33–61. <https://doi.org/10.5194/gchron-2-33-2020>
- Scholz CH (2002) *The Mechanics of Earthquakes and Faulting*. Cambridge University Press, Cambridge
- Shibata K, Ishihara S (1979) Rb–Sr whole-rock and K–Ar mineral ages of granitic rocks in Japan. *Geochem J* 13:113–119. <https://doi.org/10.2343/geochemj.13.113>
- Shibata K, Nakajima T, Sangawa A, Uchiyama S, Aoyama H (1989) K–Ar ages of fault gouges from the Median Tectonic Line in Shikoku. *Bull Geol Surv Japan* 40:661–671
- Shimizu S, Yamazaki M, Itaya T (1988) K–Ar ages of Plio–Pleistocene volcanic rocks in the Ryohaku–Hida mountains area, Japan. *Bull Hiruzen Res Inst* 14:1–36
- Shirahase T (2005) Rb–Sr whole-rock isochron ages and Sr isotopic ratios of the Nohi Rhyolite. *Monogr Assoc Geol Collab Japan* 53:119–127
- Steiger RH, Jäger E (1977) Subcommittee on geochronology: convention on the use of decay constants in geo- and cosmochronology. *Earth Planet Sci Lett* 36:359–362
- Suzuki K, Adachi M (1998) Denudation history of the high T/P Ryoke metamorphic belt, southwest Japan: Constraints from CHIME monazite ages of gneisses and granitoids. *J Metamorph Geol* 16:23–37
- Suzuki K, Morishita T, Kajizuka I, Nakai Y, Adachi M, Shibata K (1994) CHIME ages of monazites from the Ryoke metamorphic rocks and some granitoids in the Mikawa-Tono area, central Japan. *Bull Nagoya University Furukawa Museum* 10:17–38
- Tagami T (2005) Zircon fission-track thermochronology and applications to fault studies. *Rev Mineral Geochem* 58:95–122
- Tagami T (2012) Thermochronological investigation of fault zones. *Tectonophysics* 538–540:67–85. <https://doi.org/10.1016/j.tecto.2012.01.032>
- Takagi H, Iwamura A, Awaji D, Itaya T, Okada T (2005) Dating of fault gouges from the major active faults in southwest Japan; constraints from integrated K/Ar and XRD analyses. - in *Faults, fluid flow and petroleum traps*, American Association of Petroleum Geologists Memoir, 85, edited by R. Sorkhabi and Y. Tsuji, 287–301. <https://doi.org/10.1306/1033729M853139>
- Toda S, Inoue D, Miyakoshi K (1996) Paleoseismicity of the Atera Fault System, Central Japan, during the Holocene (Part 1) – Fault activity of the central to southern part and timing of the most recent faulting. *Civil Engineering Laboratory Reports*, Central Research Institute of Electric Power Industry (in Japanese with English abstract)
- Toda S (2016) *Crustal earthquakes*. In *The Geology of Japan*, edited by Moreno, T., Wallis, S., Kojima, T. and Gibbison, pp. 371–408, Geological Society, London
- Torgersen E, Viola G, Zwingmann H, Henderson ICH (2015) Inclined illite K–Ar age spectra in brittle fault gouges. *Terra Nova* 27:106–113. <https://doi.org/10.1111/ter.12136>
- Torsvik T, Doubrovine PV, Steinberger B, Gaina C, Spakman W, Domeier M (2017) Pacific plate motion change caused the Hawaiian–Emperor Bend. *Nat Commun* 8:15660. <https://doi.org/10.1038/ncomms15660>
- Tsukamoto S, Tagami T, Zwingmann H (2020) Direct dating of fault movement, in *Understanding Faults*, Elsevier, edited by D. Tanner and C. Brandes, 257–282. <https://doi.org/10.1016/B978-0-12-815985-9.00007-2>
- Ujike O, Iizuka Y, Nakano S (1992) K–Ar ages of the Ueno basaltic rocks. *J Mineral Petrol Econ Geol* 87:102–106
- Uto K, Yamada N (1985) K–Ar age of Ueno basalt, Sakashita-cho and a basalt lava south of Takayama-shi, Gifu Prefecture, central Japan. *Bull Geol Surv Japan* 36:47–52
- Uysal T, Delle Piane C, Todd A, Zwingmann H (2020) Precambrian faulting episodes and insights into the tectonothermal history of North Australia: Microstructural evidence and K–Ar, 40Ar–39Ar, and Rb–Sr dating of syntectonic illite the intracratonic Millungera Basin. *Solid Earth* 11:1653–1679. <https://doi.org/10.5194/se-11-1653-2020>
- Viola G, Scheiber T, Fredin O, Zwingmann H, Margreth A, Knies J (2016) Deconvoluting complex structural histories archived in brittle fault zones. *Nat Commun* 7:13448. <https://doi.org/10.1038/ncomms13448>
- Vrolijk P, van der Pluijm BA (1999) Clay gouge. *J Struct Geol* 21:1039–1048. [https://doi.org/10.1016/S0191-8141\(99\)00103-0](https://doi.org/10.1016/S0191-8141(99)00103-0)

- Vrolijk P, Pevear D, Covey M, LaRiviere A (2018) Fault gouge dating: history and evolution. *Clay Miner* 53:305–324. <https://doi.org/10.1180/clm.2018.22>
- Yamada N, Koido Y (2005) Nohi Rhyolite: Distribution, basement rocks, ages and lithologic features. Monograph of the Association for the Geological Collaboration in Japan 53:15–28
- Yamada N, Shibata K, Tsukuda E, Uchiyumi S, Matsumoto A, Akahane TH (1992) Radiometric ages of igneous rocks around the Atera Fault, Central Japan, with special reference to the age activity of the Atera Fault. *Bull Geol Sur Japan* 43:759–779
- Yamada R, Tagami T, Nishimura S, Ito H (1995) Annealing kinetics of fission tracks in zircon: an experimental study. *Chem Geol* 122:249–258. [https://doi.org/10.1016/0009-2541\(95\)00006-8](https://doi.org/10.1016/0009-2541(95)00006-8)
- Yamada N, Koido Y, Harayama S (2005) Volcanostratigraphy of the Nohi Rhyolite. Monograph of the Association for the Geological Collaboration in Japan 53:29–69
- Yamada K, Yasue K, Iwano H, Yamada R, Umeda K, Omura K (2012) Thermo-chronological study of the dip-slip displacement and timing of initiation of the Atera fault. *J Geol Soc Japan* 118:437–448. <https://doi.org/10.5575/geosoc.2012.0015>
- Yamasaki S, Umeda K (2012) Cooling history of the Cretaceous Toki granite in the eastern Sanyo Belt, Central Japan. *Japanese Magazine of Mineralogical and Petrological Sciences* 41:39–46
- Yamasaki S, Zwingmann H, Yamada K, Tagami T, Umeda K (2013) Constraining timing of brittle deformation and faulting in the Toki granite, central Japan. *Chem Geol* 351:168–174. <https://doi.org/10.1016/j.chemgeo.2013.05.005>
- Yuguchi T, Sueoka S, Iwano H, Izumino Y, Ishibashi M, Danhara T, Sasao E, Hirata T, Nishiyama T (2019) Position-by-position cooling paths within the Toki granite, central Japan: Constraints and the relation with fracture population in a pluton. *J Asian Earth Sci* 169:47–66. <https://doi.org/10.1016/j.jseaes.2018.07.039>
- Zwingmann H, Mancktelow N (2004) Timing of Alpine fault gouges. *Earth Planet Sci Lett* 223:415–425. <https://doi.org/10.1016/j.epsl.2004.04.041>
- Zwingmann H, Offler R, Wilson T, Cox S (2004) K-Ar dating of fault gouge in the northern Sydney basin, Australia – implications for the breakup of Gondwana. *J Struct Geol* 26:2285–2295. <https://doi.org/10.1016/j.jsg.2004.03.007>
- Zwingmann H, Mancktelow N, Antognini M, Lucchini R (2010a) Dating of shallow faults – new constraints from the AlpTransit tunnel site (Switzerland). *Geology* 38:487–490. <https://doi.org/10.1130/G30785.1>
- Zwingmann H, Yamada K, Tagami T (2010b) Timing of brittle faulting within the Nojima fault zone, Japan. *Chem Geol* 275:176–185. <https://doi.org/10.1016/j.chemgeo.2010.05.006>
- Zwingmann H, Han R, Ree JH (2011) Cretaceous reactivation of the Deokpori Thrust, Taebaeksan Basin, South Korea, constrained by K-Ar dating of clayey fault gouge. *Tectonics* 30:5015. <https://doi.org/10.1029/2010T C002829>
- Zwingmann H, Berger A, Todd A, Herwegh M (2017) Testing high-voltage electrical discharges in disintegrating claystone for isotopic and mineralogical studies: an example using Opalinus claystone. *Clay Clay Miner* 65(5):342–354. <https://doi.org/10.1346/CCMN.2017.064072>
- Zwingmann H, den Hartog SA, Todd A (2019) The effect of sub-seismic fault slip processes on the isotopic signature of clay minerals—Implications for K-Ar dating of fault zones. *Chem Geol* 514:112–121. <https://doi.org/10.1016/j.chemgeo.2019.03.034>

## Publisher's Note

Springer Nature remains neutral with regard to jurisdictional claims in published maps and institutional affiliations.